MONTE CARLO SIMULATIONS OF COMPUTED TOMOGRAPHY
FOR MEDICAL IMAGING

Kirandeep K. Gill

A thesis submitted in partial fulfillment of
the requirements for the degree of
Master of Science

Department of Physics

Central Michigan University
Mount Pleasant, Michigan
July 2013

I dedicate this work to all the people who supported
me throughout this project, without their help
I could not have come thus far.

ABSTRACT

MONTE CARLO SIMULATIONS OF COMPUTED TOMOGRAPHY
FOR MEDICAL IMAGING

by Kirandeep K. Gill

The scope of this research project is image reconstruction of different body parts with X-ray Computed Tomography (CT) and to find the radiation exposure of the patient during the CT process. Computed Tomography (CT) scanning uses special X-ray devices to generate multiple views of details of organs and/or tumors. These multiple X-ray views are reconstructed into cross-sectional images of the body using computer simulations by implementing the X-ray's feature of having different attenuation properties in different body parts. There are different methods being used to reconstruct the image of a scanned body or object. In this study we use the back projection method, which is based on Radon transform. The relevant calculations are done with FLUKA, a Monte Carlo code for particles transport simulations. Within FLUKA code the X-rays are directed on a body phantom to calculate the decrease in X-ray intensity, and this information is used for image reconstruction. Image reconstruction has a fundamental impact on the image quality and the radiation dose received by body during the scan process. Images with reasonable resolution can be reconstructed, but it may result in potential health risks. The effective dose was estimated for each reconstruction process to correlate the effect of radiation dose with image quality.

TABLE OF CONTENTS

LIST OF TABLES

LIST OF FIGURES

CHAPTER I

INTRODUCTION

Medical Imaging by X-rays

Medical Imaging is a medical field discipline. It analyzes the interaction of radiation with tissue and then it is using an appropriate approach to observe these interactions to extract clinically useful information. This information is displayed in image format. These images are then used in diagnosis and treatment of a variety of medical conditions.

Medical Imaging began in1895 with the discovery of X-rays by Wilhelm Conrad Röntgen. X-rays have the ability to visualize bones and other structures within the living body. Figure 1.1 shows the X-ray image of the wife of the discoverer of X-rays, Wilhelm Conrad Röntgen, made on December 22, 1895. Bones of her hand as well as the two rings on her finger are clearly visible.

Figure 1.1 First Radiographic Image of the Hand Wife of Discoverer of X-rays
Note: Figure taken from [1,p.4].

Earlier medical imaging utilizes the information from interaction of X-rays with tissue. If a beam of X-rays is directed on a human body, a fraction of the incoming photons will pass through it without any interaction while the other will interact with the tissue. As the beam passes through the human body, it encounters different organs and gets attenuated. The shadows in the resulting X-ray image are produced depending on the number of photons that manage to reach the detector without getting absorbed. Although such images are not very informative, they do provide some useful information about the attenuation of X-rays in different tissues. In the X-ray image, or a radiograph, a soft tissue will appear darker than a bone of equal thickness as bone absorbs most of the photons, i.e. attenuates more of X-rays. Figure 1.2 shows the chest X-ray. Dark areas have low attenuation while bright areas have high attenuation of X-rays.
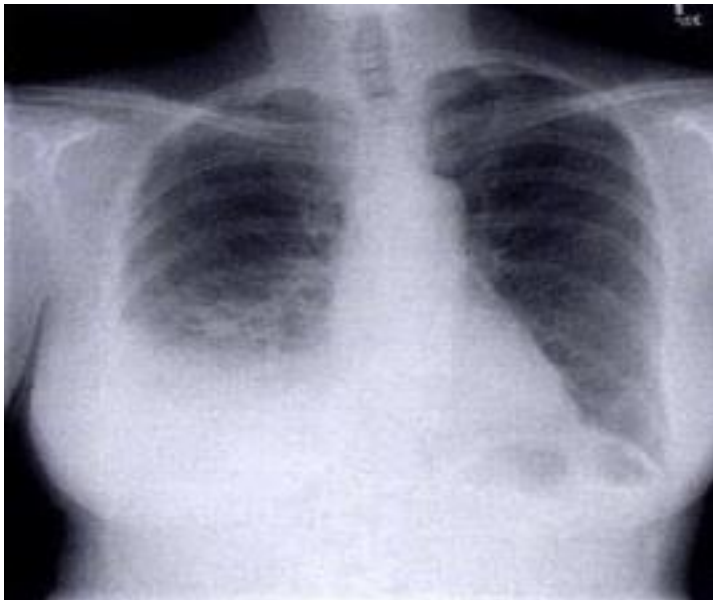
Figure 1.2 The Chest X-ray
Note: Figure taken from [1,p.5].

Computed Tomography (CT)

In radiographs or X-ray images, there is no way to detect if one object was in front of or behind another; the two overlap on the image. This means that diagnostic X-rays inherently lose depth information, and can only provide a flattened planar image of the figure [8, p.187], thus making it useful only for clinical diagnosis in cases of simple bone fractures or any other simple structural anomalies. In CT scans cross-sectional view of body anatomy is obtained, thus distinguishing many structures that overlap on a diagnostic X-ray. The word "Tomography" came from Greek word "tomo", meaning to slice, and "graphos", meaning image [6, p. 14].
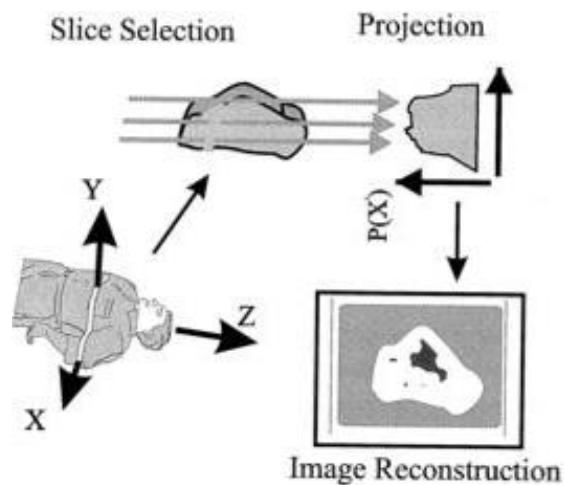
Figure 1.3 Tomographic Process
Note: The tomographic process generally consists of three steps. First a single slice is selected. Second a complete set of projections of that slice is obtained. Finally the set of projections are recombined, using a mathematical algorithm, to form a reconstructed image of the slice. Figure taken from [4,p.4].

A CT image is typically called a slice. It can be better understood by considering an analogy of a slice from a loaf of bread. Each CT slice corresponds to a certain thickness of the scanned object, like each slice of bread has certain thickness. When we stack slices of bread one

over another, the loaf of bread can be reconstituted. Figure 1.3 shows the complete tomographic process.

Similarly, a complete 3-D image of an object can be reconstructed by acquiring contiguous set of CT slices. Since Sir Godfrey Hounsfield developed the first CT scanner in 1972, this technique has become established as an essential radiological tool applicable in a wide range of clinical situations [7, p.3].

CT Scanner

A CT scanner resembles a huge doughnut from outside. It has a big cylindrical hole with diameter of roughly 70 cm. A CT scanner is a union of several component systems. It includes a table system and a gantry located in a radiation safety room. The gantry contains an X-ray source and a detector system.

Figure 1.4 Design of CT Scanner
Note: Figure taken from [2,p.12].

The patient lies on the tabletop, which is then inserted to the gantry hole (Figure 1.4). The X-ray source and the detector are then rotated around the areas to be scanned. After finishing the scanning process, a computer is used to control the data acquisition, the image reconstruction and its display.

CT Imaging Principle

In CT imaging X-rays are directed at an object from multiple orientations, and their decrease in intensity along a series of linear paths is measured. This decrease in intensity is given by Beer's law [24] as a function of X-ray energy, path length, and linear attenuation coefficient of material. The simplest form of Beer's law is:

$$I = I_o \exp[-\mu(E)x] , \qquad (1.1)$$

where I and I_o are the initial and final intensity of monochromatic X-ray beam, $\mu(E)$ is the linear attenuation co-efficient of the material where E signifies the energy dependence, and x is the length of X-ray path. For more than one material, the equation can be rewritten as:

$$I = I_o \exp[\sum_i(-\mu_i\, x_i)], \qquad (1.2)$$

where 'i' material number. Figure 1.5 shows the complete assembly of a CT scanner. The X-ray tube is rapidly rotated 360° around the patient. The X-rays passing through the plane of finite-thickness cross section of the body get attenuated at different rates by different tissues and the detectors on the other side collect these measurements of attenuation. The system uses this data to reconstruct a digital image of the cross-section.
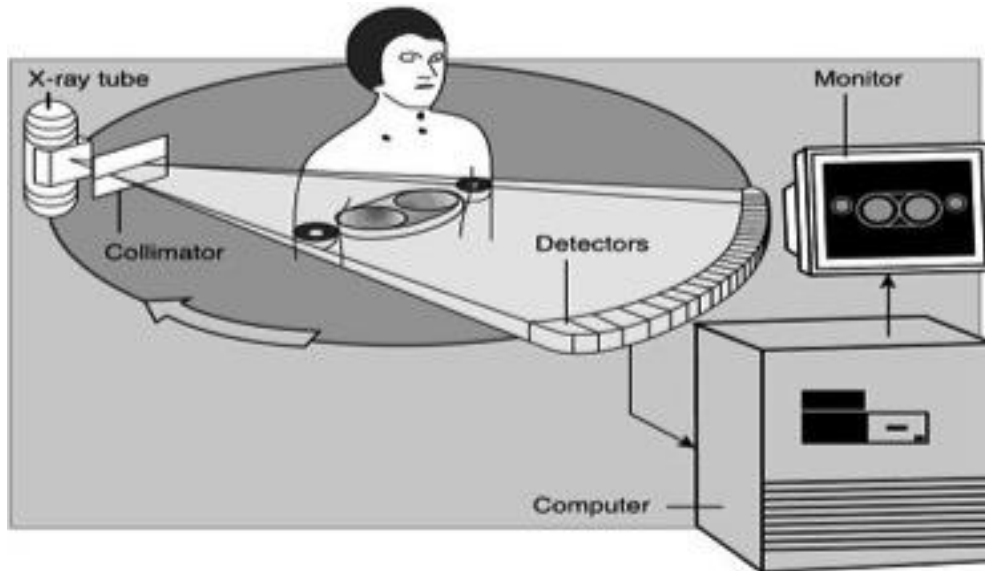
Figure 1.5 Schematic Illustration of CT Imaging Operation
Note: Figure taken from [6,p.15].

Each pixel in the image represents the measurement of the mean attenuation that extends through the thickness of section. Each attenuation measurement is called a *ray sum* because attenuation along a specific straight-line path through the patient from the tube focal spot to a detector is the sum of the individual attenuations of all materials along the path [6, p.14]. A series of X-ray projections, which are made across the different regions of body, are collected in a particular direction. A complete data set to reconstruct images requires projections collected in different directions at rotational intervals of 1° or less around the cross-section. After getting the complete projection data, a specialized algorithm is needed to reconstruct the distribution of X-ray attenuation. Back-projection algorithms effectively trace backwards the X-rays path to get reconstructed images.

CHAPTER II

MEDICAL IMAGING BY COMPUTED TOMOGRAPHY

Reconstruction Method

A variety of reconstruction methods exist to estimate the cross-sectional distribution of the attenuation coefficients. The knowledge of basic elements of reconstruction method can help to reconstruct images with the lowest possible noise without sacrificing image accuracy and spatial resolution. The two major categories of reconstruction techniques are: Analytic and Iterative reconstruction techniques. Algebric Reconstruction Technique (ART), Simultaneous Iterative Reconstruction Technique (SIRT), and Iterative Least Squares Technique (ILST) are the main examples of Iterative reconstruction techniques, whereas 2-D Fourier analysis and Filtered back projection are Analytic reconstruction techniques. Iterative reconstruction techniques are computationally more expensive than Analytic reconstruction techniques. Therefore, Analytic reconstruction methods are mostly used for reconstruction purposes. The most popular and frequently used reconstruction method in medical CT systems is the filtered back projection method, an analytic reconstruction technique.

Filtered Back Projection

Filtered back projection can be both used for parallel-beam and fan-beam modes. Figure 2.1 illustrates both parallel and fan beam configurations for projecting X-rays. An X-ray point source is used in fan beam, while in parallel configuration a rectangular beam is used and width of beam is limited by the width of object.
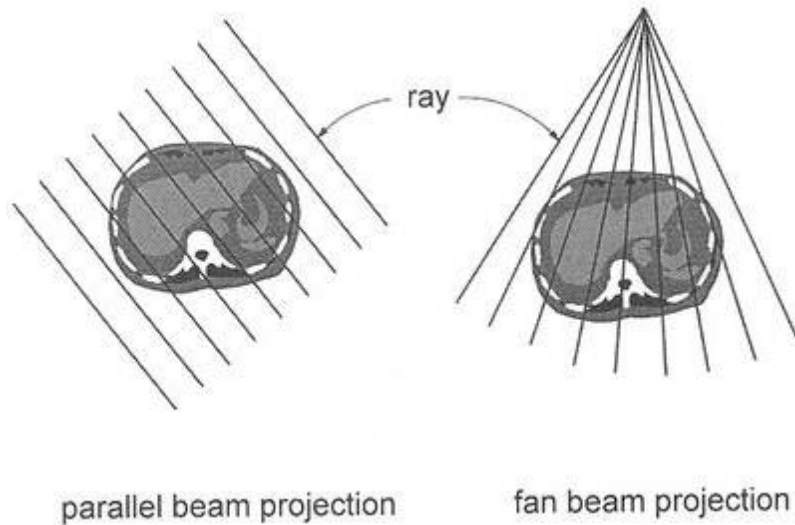
Figure 2.1 Parallel and Fan Beam Projections of X-ray Beam in CT
Note: Figure taken from [29].

The basic concept behind filtered back projection is relatively easy to understand. Figure 2.2 illustrates the idea behind back projection, which is to obtain the rough approximation of original image by running the projections backward.

As already mentioned, when X-rays pass through the body they get attenuated. The detectors on the opposite side of X-ray source measures the attenuated X-ray intensity transmitted through the body section. Knowing these X-ray intensity values, the line sum of all X-ray absorption coefficient corresponding to that particular X-ray beam can be computed. As shown in Figure 2.2 (a), the numbers along detectors show the line-sum of X-rays. After getting values for forward projection, backward projection can be employed. Backward projection, as the name suggests, tracks back the X-ray path from each detector. An absorption value based on sum of absorptions from each detector is assigned to each region of overlap between such back projections, providing a matrix of all X-ray absorptions, which can be displayed as a gray scale image. Back projection itself does not provide clear images. However, if forward projections are first subjected to a mathematical process called filtering, it can reduce the artifacts in back

projection method. This process is called Filtered backward projection or Filtered back projection.
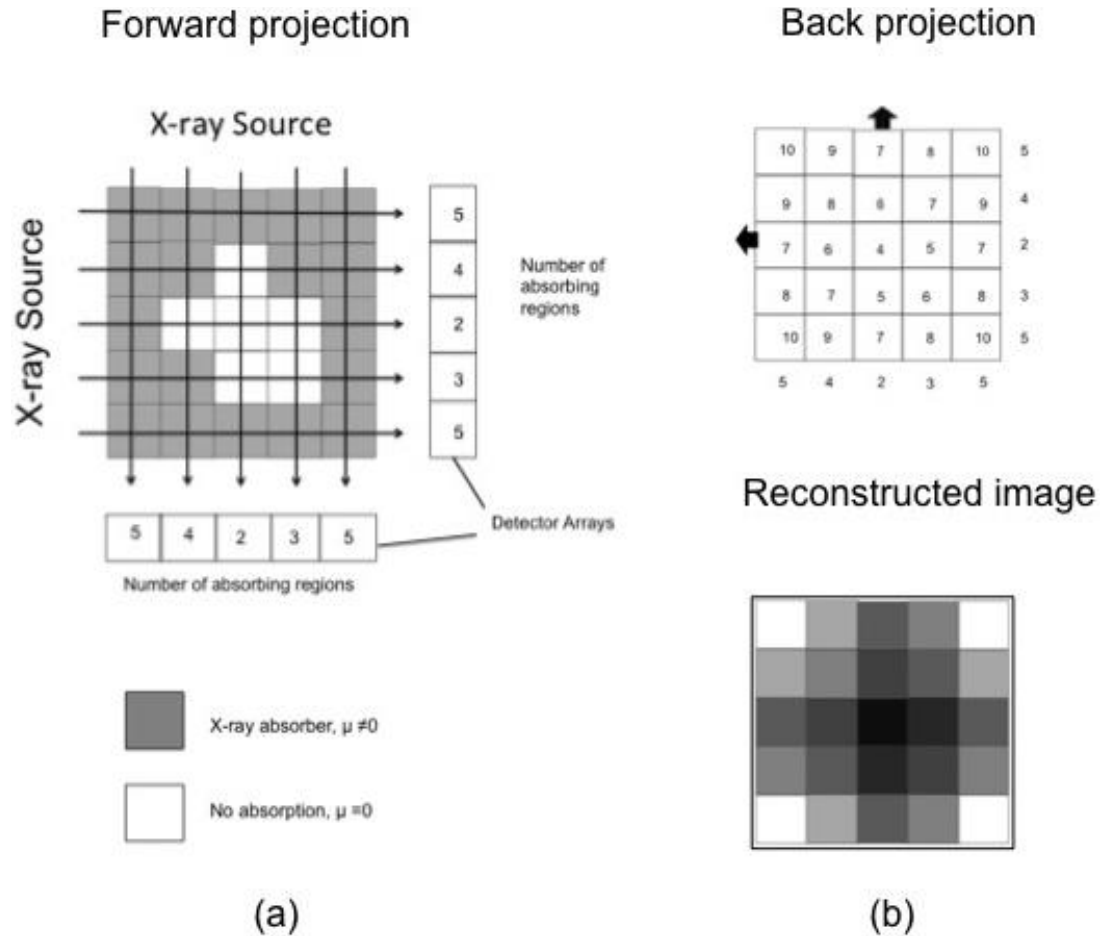
Figure 2.2 Filtered Back Projection Method
Note: Filtered back projection in the production of CT images. The tissue being scanned is represented by a gray scale indicating its absorption coefficient. (a) Creation of forward projections for two source and detector orientations. (b) Reconstruction of the original absorber's cross-section, using back projection. Figure taken from [8,p.242].

Projection Data

Projection data values correspond to the attenuation values of objects, which are measured across the patient in a particular direction in the section plane. For a narrow, mono-energetic beam of X-rays, Beer's law of absorption can be used to determine the projection data values:

$$I = I_o e^{-\mu x},$$ (2.1)

Or

$$\frac{I}{I_o} = e^{-\mu x},$$ (2.2)

where I is the intensity of transmitted beam, I_o is the initial intensity of the beam transmitted, μ is linear attenuation co-efficient of the material, and x is the thickness of body (absorber).
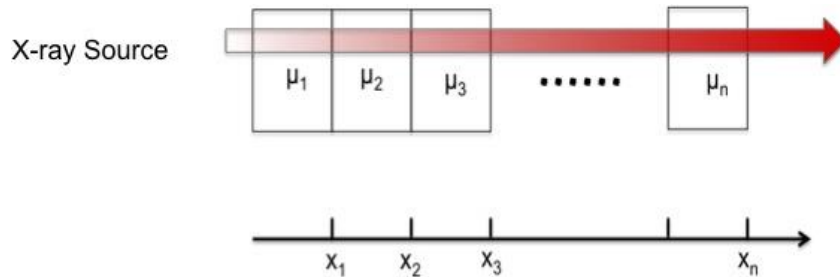
Figure 2.3 Attenuation of X-ray Beam while Passing through a Number of Consecutive Non-Homogenous Absorbers
Note: Figure taken from [2,p.47].

If there are two or more consecutive non-homogenous absorbers (Figure 2.3), with thickness x_1, x_2, x_3, ...x_n and respective attenuation co-efficient μ_1, μ_2, μ_3, ... μ_n, the overall transmitted intensity is:

$$\frac{I}{I_o} = e^{-\mu_1.x_1} * e^{-\mu_2.x_2} * e^{-\mu_3.x_3} ... e^{-\mu_n.x_n},$$

10

Or

$$\frac{I}{I_o} = e^{-\sum_{i=1}^{n} \mu_i \cdot x_i},$$ (2.3)

where μ_i and x_i are the linear attenuation co-efficient and thickness of the ith component,

respectively.

Considering a two dimensional section through an object of interest, the integral

equivalent of above equation can be written as:

$$\frac{I}{I_o} = e^{-\int \mu(x,y)ds},$$ (2.4)

where $\mu(x, y)$ is linear attenuation coefficient with (x, y) as Cartesian co-ordinates specifying

location within the section.

The objective of reconstruction program is to determine $\mu(x, y)$ distribution, from a

number of intensity measurements through the section. This can be found by rearranging above

equation:

$$-\ln\left(\frac{I}{I_o}\right) = \int \mu(x,y)ds.$$ (2.5)

This is the basis of Radon transformation, and it represents the projection data. Radon transform

is discussed in more detail in section 2.1.3.

Mathematical Basis of Reconstruction Method: Radon Transform

Mathematical basis of image reconstruction by back projection method is Radon

transform. The Radon transform is a mathematical technique consisting of the integral of a

function over straight lines, and its inverse is used to reconstruct images in medical computed

tomographic scans.
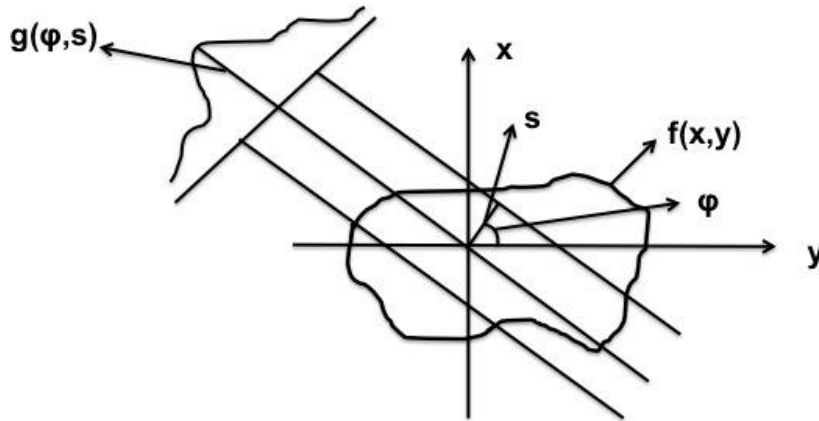
Figure 2.4 Radon Transform Concept
Note: Parallel lines represent the X-rays passing through the body. $g(\varphi,s)$ represents the line
integral of image intensity, $f(x,y)$, at angle φ and distance s from the center of co-ordinate system.
Figure taken from http://www.clear.rice.edu/elec431/projects96/DSP/bpanalysis.html

For a given angle φ, the line integral of function $f(x, y)$ (Figure 2.4) is given by:

$$g(\varphi, s) = \int_l f(x, y)dl, \tag{2.6}$$

where $g(\varphi, s)$ is 1-D projection data at angle φ and distance s, where φ is the angle at which the

gantry is rotated around the body, and s is the distance of a parallel X-ray from origin.

All the points on any line (X-ray) satisfy the equation for straight line:

$$x*sin(\varphi) - y*cos(\varphi) = s . \tag{2.7}$$

Therefore equation (2.6) can be rewritten as:

$$g(\varphi, s) = \iint f(x, y)\delta(x * sin\varphi - y * cos\varphi - s) \, dx \, dy. \qquad (2.8)$$

The collection of this function $g(\varphi, s)$ at all angles of rotation φ and at all distances s is called Radon transform of function $f(x, y)$. The Radon transform data is often called a sinogram due to its characteristic sinusoid shape.

To reconstruct the original image from the projection data, the inverse Radon transform is used. Inverting the Radon transform means summing up Radon projections along all angles passing through the same body elements.

Mathematically, the inverse Radon transform is given as:

$$\tilde{f}(x, y) = \int_0^\pi g(\varphi, x * sin\varphi - y * cos\varphi) d\varphi. \qquad (2.9)$$

Figure 2.5 shows the Radon and inverse Radon transform of Shepp-Logan phantom [28]. Shepp-Logan phantom is a standard test image that serves as model of the human head to test the image reconstruction techniques.

(a)   (b)   (c)
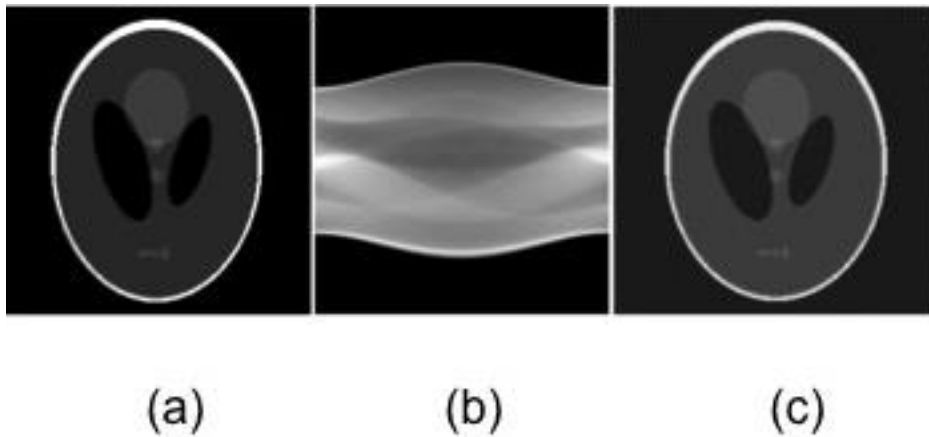
Figure 2.5 (a) Shepp Logan Phantom (b) Radon Transform (c) Inverse Radon Transform
Note: Figure taken from http://en.wikipedia.org/wiki/Radon_transform

13

Radiation Dose in CT Exam: Effective Dose

Over the past few decades, there has been enormous growth in the number of diagnostic medical procedures utilizing ionizing radiation. Although most of these diagnostic procedures undoubtedly have tremendous and unbelievable benefits, however, these are always accompanied by some kind of radiation risks due to ionizing radiation. It is very important to have some idea of the magnitude of radiation dose associated with these procedures. When ionizing radiation penetrates the human body/object, some of its energy is deposited in the body. The energy absorbed by the body or object from the exposure to radiation is called radiation dose and if it is measured as energy deposited by the ionizing radiation per unit mass of the medium, it is called absorbed dose. Absorbed dose is measured in kilogram/joule, called Gray (Gy) in S.I. Radiation exposure can be from different natural sources or different diagnostic procedures in medical science. The benefits of medical imaging usually overweigh the risks of radiation-induced cancer. However, a high-level radiation exposure to the whole body may cause potential health risks. To avoid these health risks certain effective dose limits are set for both general public and radiation workers. Effective dose measures the cancer risks due to non-uniform irradiation of body due to ionizing radiation. It is explained in detail later in this section. Table 2.1 shows the annual effective dose from different sources and dose limit for general people and people working in radiation field.

Table 2.1 Typical Values of Annual Effective Dose Encountered

Source of Exposure	Annual Effective Dose (mSv)	Comments
Natural Background	~1	Terrestrial+cosmic+internal
Radon (daughters)	~2	Individual Doses Very Variable
Radiation Work Limit	20	ICRP and NCRP
Highest Worker Doses	~5	Typical Effective Dose to IR Fellow
Public Dose Limits	1	Excludes Background and X-rays
Radiation Worker Conceptus	5	No More than 0.5/Month

Note: Source- Table taken from [13].

Different diagnostic procedures have different radiation exposures. Many of them have radiation exposure similar to what we have from background radiation. Table 2.2 shows that a few diagnostic exposures are higher than background exposure.

Table 2.2 Typical Effective Doses in Diagnostic Radiology

Imaging Modality	Examination Type	Representative Effective Dose (mSv)
Radiography	Skill	~0.1
	Chest	~0.05
	Abdomen	~0.4
Fluoroscopy	Barium Swallow	~1
	Barium Meal	~3
	Barium Enema	~5
CT	Head	~1
	Chest	~5
	Cardiac	~10
Nuclear Medicine	Abdomen/Pelvis	~5
	Planar Imaging/SPECT	~5
	Positron Emission Tomography	~10

Note: Source- Table taken from [12].

Radiation dose is not same for the whole body; different tissues and organs have different radiation sensitivities. For example, bone absorbs more radiation than soft tissue. So, for non-uniform irradiation, like in CT scan, one needs to consider an effective dose. The effective dose in radiation protection and radiology is a measure of the cancer risk to the whole organism due to ionizing radiation delivered non-uniformly to the part(s) of its body [12]. On the other hand, the quantity that takes into account the damaging properties of different types of radiation is called equivalent dose (H_T). When radiation is absorbed in living matter, biological effects observed will not necessarily be equal. It depends on the type of radiation. Equivalent dose is the absorbed dose weighted for the degree of the effect of different radiation. A radiation-weighing factor (W_R) is used to estimate the relative biological effectiveness of the radiation [14]. Equivalent

dose can be calculated by multiplying the absorbed dose by specified radiation weighing factor (W_R):

$$H_T = \sum_R W_R . D_{T,R},\qquad(2.10)$$

where H_T is equivalent dose absorbed by organ/tissue, $D_{T,R}$ is absorbed dose by radiation type R in tissue T, W_R is radiation-weighing factor. Equivalent dose is measured in Sievert (Sv). Table 2.3 summarizes the radiation weighing factors according to International Commission of Radiological Protection (ICRP) recommendations to represent effectiveness of particular radiations.

Table 2.3 Radiation Weighing Factors (W_T)

Radiation	Energy	W_R
X-rays, gamma rays, Beta rays, muons		1
Neutrons	< 1MeV	$2.5 + 18.2 {}^* e^{-[\text{In}(E)]^2}/6$
	1 MeV -50 MeV	$5.0 + 17.0 {}^* e^{-[\text{In}(2.E)]^2}/6$
	< 50 MeV	$2.5 + 3.25 {}^* e^{-[\text{In}(0.04.E)]^2}/6$
Protons, charged pions alpha rays,		2
Nuclear fission products, heavy nuclei		20

Note: Source - http://en.wikipedia.org/wiki/Equivalent_dose

Effective dose (E) was introduced by ICRP to provide a summation of radiation doses to the tissues and organs for radiation protection [13]. Effective dose of radiation can be obtained by summing individual organ equivalent dose H_T multiplied by the corresponding tissue weighing factors

$$E = \sum_T W_T . H_T,\qquad(2.10)$$

where E is effective dose for entire organism, H_T is the equivalent dose for tissue T, W_T is tissue-weighing factor, T is tissue or organ. The tissue weighing factors, W_T, estimate the sensitivity of

various organs for the exposed radiation. Table 2.4 summarizes the various tissue weighing

factors as prescribed by ICRP over the years. The effective dose is also measured in the units of

Sievert (Sv).

Table 2.4 Weighting Factors for Different Organs

Organ	Tissue Weighting Factors, W_T		
	ICRP 30[136] 1979	ICRP 60 [13] 1991	ICRP 103 [16] 2008
Gonads	0.25	0.20	0.08
Red Bone Marrow	0.12	0.12	0.12
Colon		0.12	0.12
Lungs	0.12	0.12	0.12
Stomach		0.12	0.12
Bladder		0.05	0.04
Breasts	0.15	0.05	0.12
Liver		0.05	0.04
Oesophagus		0.06	0.04
Thyroid	0.03	0.01	0.01
Skin		0.01	0.01
Bone Surfaces	0.03	0.01	0.01
Salivary Glands			0.01
Brain			0.01
Remainder	0.30	0.06	0.12

Note: Source- UNSCEAR-2008 Annex A page 40, table A1, retrieved 2013-06-2

CHAPTER III

PHYSICS BEHIND COMPUTED TOMOGRAPHY

Interaction of X-rays with Matter

Imaging with X-rays depends on the number of photons emitted from an X-ray tube, that traverse a patient's body undeviated by interactions with atoms of the body [4, p.54]. As X-rays pass through the matter, beam intensity attenuates. This attenuation in beam intensity results from the interaction of X-ray photons with the atoms in absorber (patient). X-ray photons are either absorbed (by transfer of energy from X-ray photons to absorbing material), or scattered (X-ray photons are redirected by interaction with the scattering material) within the body. The efficiency of the processes by which absorption or scattering occurs depends on the energy of photons and the properties of body tissues through which they travel.

Theoretically there are many processes that can occur when X-rays interact with matter, but only three of these are important in diagnostic procedures:

a) Photoelectric effect.

b) Compton effect.

c) Pair production.

The graph in Figure 3.1 illustrates which process dominates depending upon the energy of photons and absorption probability of materials. The probability of photoelectric effect is higher at lower photon energies and drops at higher photon energies. At higher photon energies Compton effect becomes more prominent. At energies greater than 1.02 MeV the phenomenon that plays an important role in particle interaction is pair production.
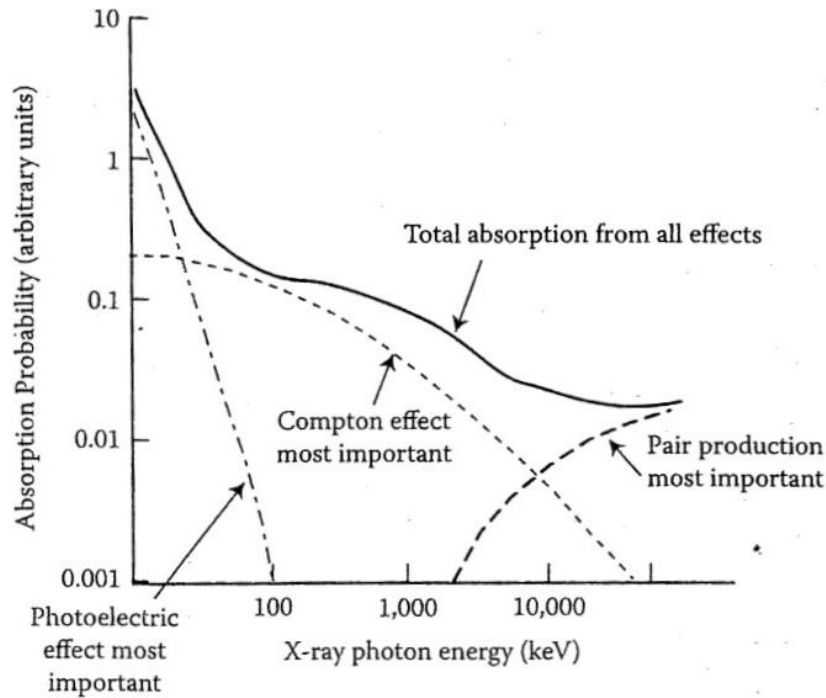
Figure 3.1 Absorption of X-rays in Water as a Function of Energy, Indicating the Separate Contributions Due to the Photoelectric Effect, Compton Effect, and the Pair Production Note: Figure taken from [8,p.194].

Photoelectric Effect

Photoelectric effect dominates the absorption of X-rays with energies below approximately 25 keV. In this phenomenon, an incoming photon interacts with a tightly bound electron inhabiting an innermost orbital of an atom [8,p.192]. Sometimes, the X-ray photon is completely absorbed in the interaction, which gives the electron enough energy to escape the orbital and hence become completely free. These ejected electrons are called photoelectrons. The kinetic energy of photoelectron is given as:

$$K.E. = E_x - P, \qquad (3.1)$$

where K.E. is kinetic energy of photoelectrons, E_x is the energy of incident X-ray photons, and P

is the ionization potential of the atoms i.e. the energy required to remove the electron from its

orbital.
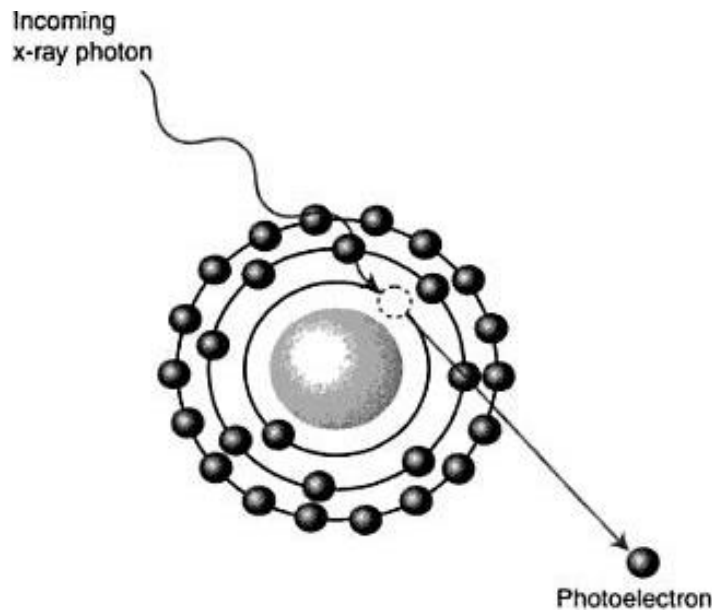
Figure 3.2 The Photoelectric Effect
Note: An X-ray photon interacts with an atom within the body, resulting in the excitation of an
inner-orbital electron. The resulting photoelectron is free to travel, while the X-ray photon is
entirely absorbed. Figure taken from [8, p.192].

Photoelectrons are free to travel throughout the body, but their energy is reabsorbed very

soon, so they travel very short distances. Meanwhile, the vacant orbital is refilled by capture of

another electron. The energy released during the capture usually shows up as a photon called

characteristic X-ray. This characteristic X-ray photon can contribute to the scattering if it escapes

the body.

The probability of absorption of X-ray photons depends on the atomic number, Z, of

chemical elements in the absorbing material. The likelihood of photoelectric effect increases as

the cube of atomic number, Z^3 [8,p.193]. Therefore, photoelectric effect is most likely to occur in

20

materials that have large atomic number. For example, heavy metals such as lead (Z=82) are good absorbers of X-rays, so they can be used in, e.g., lead aprons for shielding parts of the body during X-ray diagnosis [8,p.193].

The average value of atomic number, Z, decides the probability of absorption by photoelectric effect. For soft tissue the average value of atomic numbers of various elements is $Z_{soft\ tissue}$=7.4 and for bone Z_{bone}=12.7, which means that soft tissue has less probability of absorbing X-rays by photoelectric effect, whereas bone has much higher probability.

Table 3.1 Attenuation Coefficient at 60 keV and Density for Some Materials Important to Medical X-ray Imaging

Absorbing Material	Attenuation Coefficient At 60 keV, μ (cm^{-1})	Density ρ (g/cm^3)
Fat	0.1788	0.91
Soft tissue other than fat (muscle, body fluids)	0.2045	1.00
Water	0.2055	1.00
Brain	0.2061	1.00
Air	~3 X 10^{-4}	0.00129
Bone	0.466 to 0.548	1.65 to 2.0

Note: Source- Table taken from [8, p.196].

Material density is another factor that influences how many atoms the X-ray encounters when it passes through a given thickness of material. So, a denser material is better absorber of X-rays than a less dense material.

Compton Effect

As the X-ray photon energy become above 25 keV, a different process called Compton effect becomes more important. In this process the X-ray photon collides with the loosely held outer orbital electron. Exciting such an electron requires less energy than for the photoelectric effect, due to which, photon-electron interactions in Compton processes are significantly

different than in photoelectric effect. In fact, the Compton effect is analogous to having a pool

ball (the X-ray photon) hit another pool ball (the electron, acting as though it's free of its

associated atom), setting the second ball in motion while its recoiling [8,p.193]. Like a pool ball

hits multiple other balls, a single X-ray photon can also undergo multiple encounters. Photon

loses energy during each encounter and travels in a different direction than the original X-ray

photon, as illustrated in Figure 3.3. This is called Compton scattering.
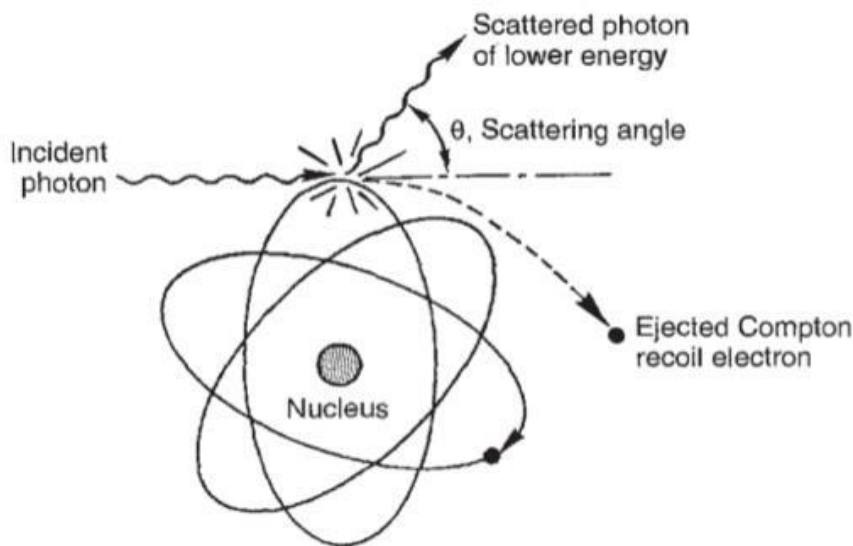
Figure 3.3 The Compton Effect
Note: An incident X-ray photon transfers energy to an outer shell electron, which leads to the
ejection of the electron and a scattered X-ray photon. Figure taken from [19,p.78].

The energy of the scattered photon is given by:

$$E' = \frac{E}{1+\left(\frac{E}{m_0 c^2}\right)(1-cos\theta)},$$
(3.2)

where E is the energy of the incoming X-ray photon, $E^{'}$ is the energy of scattered photon, c is the

speed of light, m_0 is the rest mass of electron, and θ is the angle of scattering.

Compton scattering is independent of atomic number of absorber. Only the thickness and the density of absorber are important. Compton scattering can also corrupt the eventual image because of the loss of directional information.

Pair Production

Pair production occurs when X-ray energy is greater than 1.02 MeV. In this process, an electron and a positron are created with annihilation of the X-ray photon. Pair production is not a very significant process at X-ray energies involved in computed tomography.

CHAPTER IV

MONTE CARLO METHOD FOR PARTICLE TRANSPORT SIMULATION

Monte Carlo Method

Monte Carlo, in its simplest form, can be seen as numerical technique of solving mathematical problems by simulation of random variables. It is a highly flexible and widely used numerical procedure that can be applied to a wide range of problems, for example, tossing of a coin, radioactive decay, particle transport etc. Random variables and probability statistics are two major components of Monte Carlo methods. A variable is considered random if we do not know that variable's value, but we do know the values it can assume. Monte Carlo methods enable simulation of any problem whose development is influenced by random factors. To apply Monte Carlo methods it is not necessary that a problem should be expressed explicitly as an integral, but it can be estimated by simulating the problem.

In my research project I am using Monte Carlo methods to simulate the particle transport problem. Particle transport refers to the transport of small particles, such as protons, electrons, neutrons, photons etc. within some host medium such as air, water, earth's atmosphere, or human body. A Monte-Carlo particle transport calculation simulates a finite number N of particle histories. A history begins by randomly selecting a particle's initial position, energy, and direction. As particle travels, a sampling is performed to determine random values for distance to the next interaction, type of interaction, scattering angle, energy change and so on. During some interactions, secondary particles are created. After the original particle finishes its history, these secondary particles are processed to create new histories [25].

After each history is terminated, its contribution is added to estimate the quantity of interest. If z_i is the contribution from each history, the estimated total contribution from N histories is:

$$< z > \simeq \bar{z} = \frac{1}{N}\sum_{i=1}^{N} z_i \tag{4.1}$$

For N number of histories, the error of calculation is proportional to $\sqrt{D/N}$, where D is some constant. Hence, to decrease the error, it is necessary to increase the number of histories.

FLUKA: Code for Particle Transport Simulation

In my research work to simulate particle interaction and transport, I used FLUKA code. FLUKA, a general-purpose tool, is a fully integrated Monte Carlo simulation package. It has a very wide range of applications covering calorimetry, dosimetry, detector design, neutrino physics, radiotherapy, etc. FLUKA can simulate the interaction and transport of 60 different particles, including photons and electrons of energy 1keV to thousands of TeV, with high accuracy [21].

The structure of FLUKA input file (as discussed in Appendix A) consists of different cards. Cards are used to define source, geometry, materials, output (score), etc. FLUKA code is facilitated with an advanced graphical user interface (GUI), called "flair", to make editing of FLUKA input files simple for the users. Flair has many other important features: it can be used to visualize and edit the input geometry using interactive geometry editor, it provides immediate debugging information, it has materials library, which makes it very easy to assign different materials to different bodies. There is another graphical tool available, Simple Geo that can be

25

used to visualize the input geometry with certain limitation. For example, the source cannot be

visualized with this tool, the rotation of body at different angles cannot be checked, and the

detector binning can be visualized in only one direction.

Method

The computed tomographic process is simulated using the output of FLUKA simulations.

FLUKA has no direct application in computed tomographic image reconstruction. In my

research, I wanted to establish a relation between FLUKA output and image reconstruction by

computed tomography. For this purpose, I used a simple simulation set-up that consists of a body

phantom in the center, a rectangular X-ray beam on one side of the body phantom, and an array

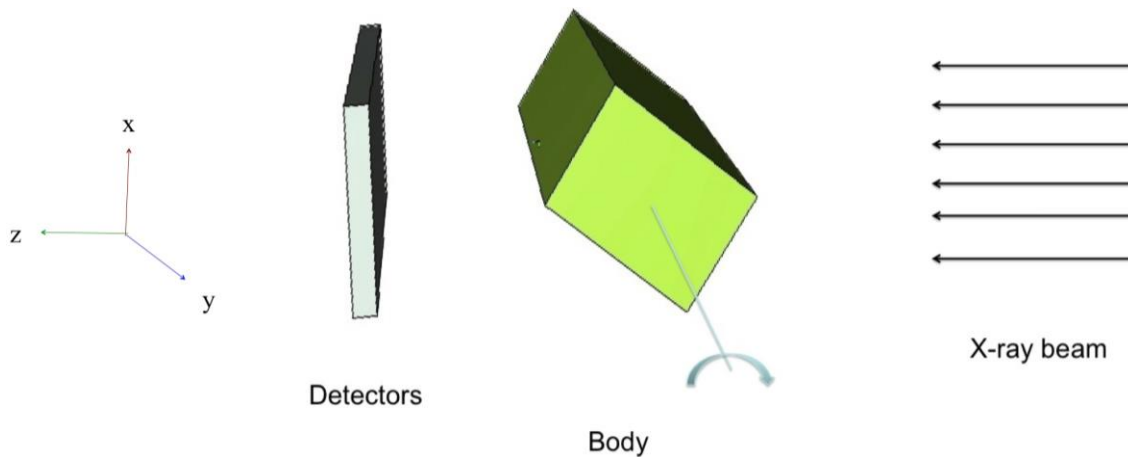of detectors on the other side (as shown in Figure 4.1).

Figure 4.1 C.T. Scan Process
Note: The X-ray source and detectors are fixed and body is rotated along y-axis.

First, I simulated a very simple geometry with two small cubes inside a bigger cube

(Appendix C). After getting a clear image for the first example, a more complex geometry was

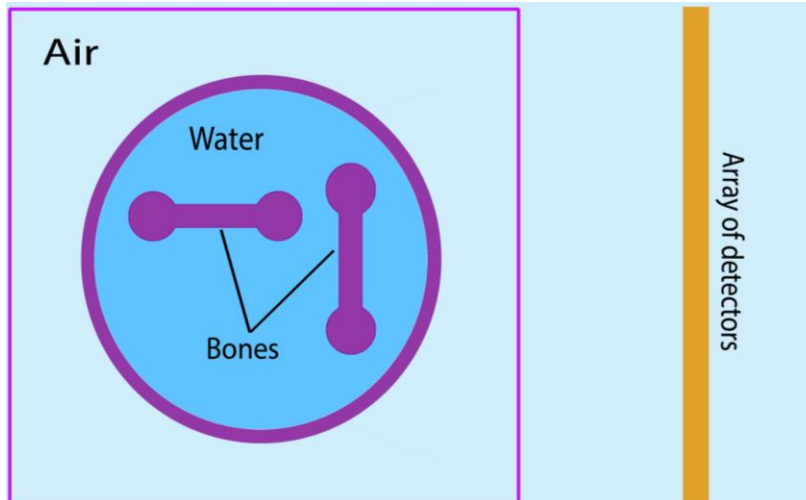simulated as shown in Figure 4.2.

26

Figure 4.2 Input Geometry for Image Reconstruction Process

In Figure 4.2 bones are simulated using the geometry cards and material cards of FLUKA input, as discussed in Appendix A. Bones are surrounded by water to simulate human body, as 70% of human body is water. X-rays of energy 80-140 keV are used in the CT process. For my simulations I used 140 keV X-rays. In practical CT applications three-dimensional images of internal organs are reconstructed, but in my project I am reconstructing only cross-sectional image of a thin slice of 1 centimeter. After stacking these thins slices, a three-dimensional image can be reconstructed easily. Silicon is used for the detector material. To simulate the array of Silicon detectors 168 bins in x direction and 4 in y direction are used, thus making the pixel size 0.25 cm.

In practical CT processes the gantry (X-ray source and detector) is rotated around body, but due to limitation of viewing X-ray source in Simple Geo, I rotated the body instead. The detectors score number of photons left after the X-ray beam passes through the body and get attenuated. The initial number of photons is the input parameter for FLUKA. Using the equation for attenuation of beam (Equation 2.5) one gets:

$$-ln\frac{N}{N_0} = \int \mu(x,y)dl \ , \tag{4.1}$$

where N is number of photons scored in detectors, N_o is initial number of photons, μ is

attenuation coefficient. The left hand side of equation (4.1) is calculated using a simple

FORTRAN code for each angle of projection from 0-180^0 with the angle increment of 1^0.

The output of detectors (*-lnN/N$_o$*) is stacked over one another for all angles to get the

image matrix (Appendix E). The plot of image matrix gives a sinogram. To reconstruct the

original image, the inverse Radon transform is used. I used Mathematica software to calculate

the inverse Radon transform to get original image.

In the next part of my research, I tried to estimate the radiation risks in the computed

tomographic process, by estimating the effective dose for the geometry used for image

reconstruction (Figure 4.2). The effective dose is very helpful in providing approximate

indication of potential detriment from ionizing radiation, and it is mostly used as one parameter

to evaluate the appropriateness of assessing the risks of ionizing radiation. The effective dose

takes into account which tissue has absorbed energy from radiation. The effective dose was

calculated by using "AUXSCORE" card (Appendix D) in FLUKA code. The FLUKA code

provides a user-routine "deq 99.f" to convert fluence into effective dose, where fluence is the

total number of particles that intersect a unit area in a particular time interval. The conversion

coefficients used for this purpose are based on fits to values for discrete energies, and are given

for different incident particles, such as protons, electrons, neutrons, photons, etc. [27]. The

detailed procedure of finding effective dose is explained in the appendix D.

CHAPTER V

RESULTS AND DISCUSSION

Image reconstruction has a fundamental impact on image quality and on radiation dose during the scanning process. It is always desirable to reconstruct images with the lowest possible noise without sacrificing image accuracy for a given radiation dose [17]. So, to illustrate this trade off between image quality and radiation dose in computed tomography, I ran the same simulation three times with different number of histories (initial number of photons) for image reconstruction. Then I calculated the effective dose for these respective numbers of histories.

Image Reconstruction

After the projection data has been collected, the image matrix was created from the output of the detector for each simulation set-up. A simple Fortran code was used to create the image matrix from projection data. The next step is to plot the image matrix, i.e. the output of detectors, $[-ln(N/N_0)]$, versus angle φ and displacement s. Mathematica software is used to plot the image matrix.

First, I started with 1E7 initial number of particles. The simulation set-up used is shown in Figure 4.2. The sinogram obtained by plotting the matrix is shown in Figure 5.1.
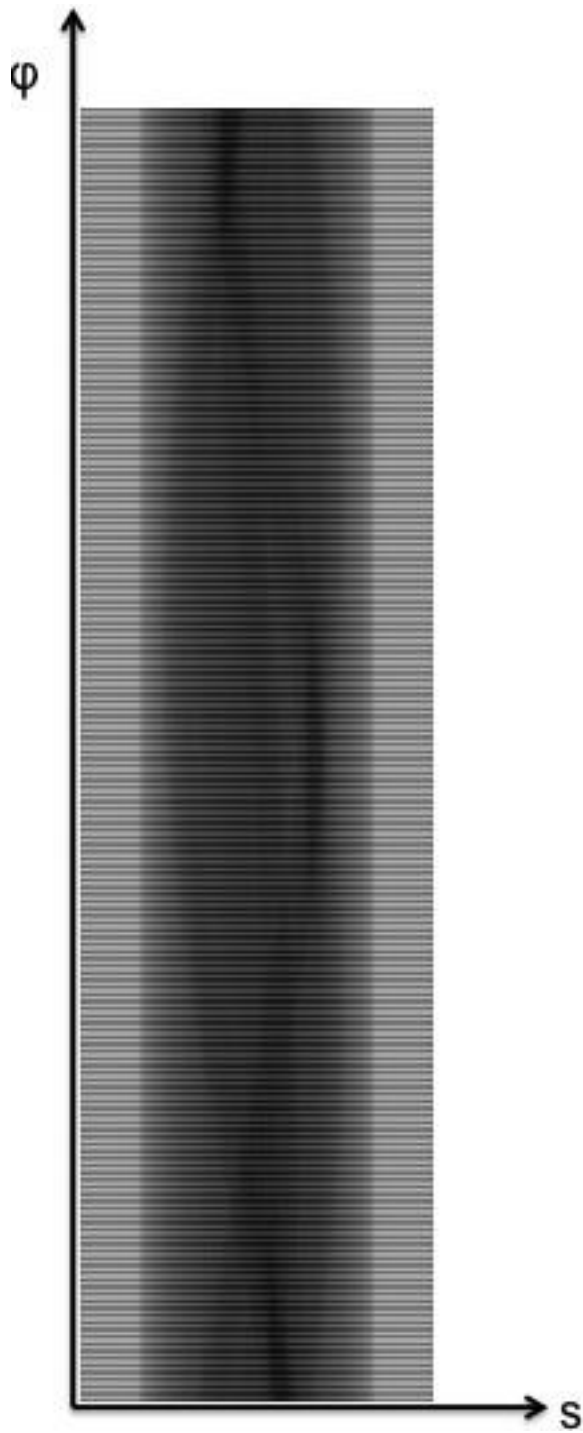
Figure 5.1 Plot of Function $-lnN/N_o$ (Radon Transform) versus Displacement s and Angle φ for N Equal to1E7
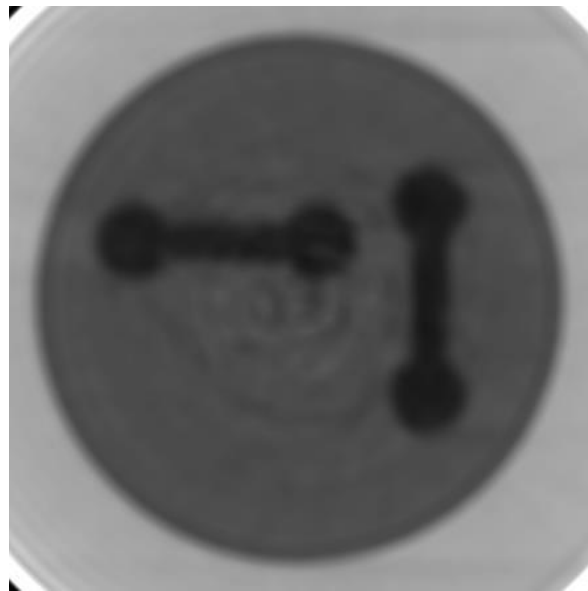

Figure 5.2 Cross-Sectional Image of Body After Using Inverse Radon Transform for Figure 5.1

Lighter regions indicate higher values, i.e. higher attenuation, and darker regions indicate lower values. The blurred sine waves in the sinogram represents the Radon transform of different objects at different angles of input geometry. The original image is reconstructed using Mathematica software. Mathematica has a built in function that calculates the inverse Radon transform and return the original image. Figure 5.2 shows the reconstructed original image.

Angle φ in the Figure 5.1 is the angle of projection that varies from -90^0 through 0^0 to 90^0. Distance s is the projection displacement plotted horizontally. Cross-sectional image in Figure 5.2, returned by Mathematica is always a square image, having each side equal to diagonal of original image.

For the second simulation I increased the number of particles to 5E7 and I repeated the same procedure to reconstruct the image. Radon and inverse Radon transforms of this simulation are shown in Figure 5.3 and Figure 5.4 respectively.
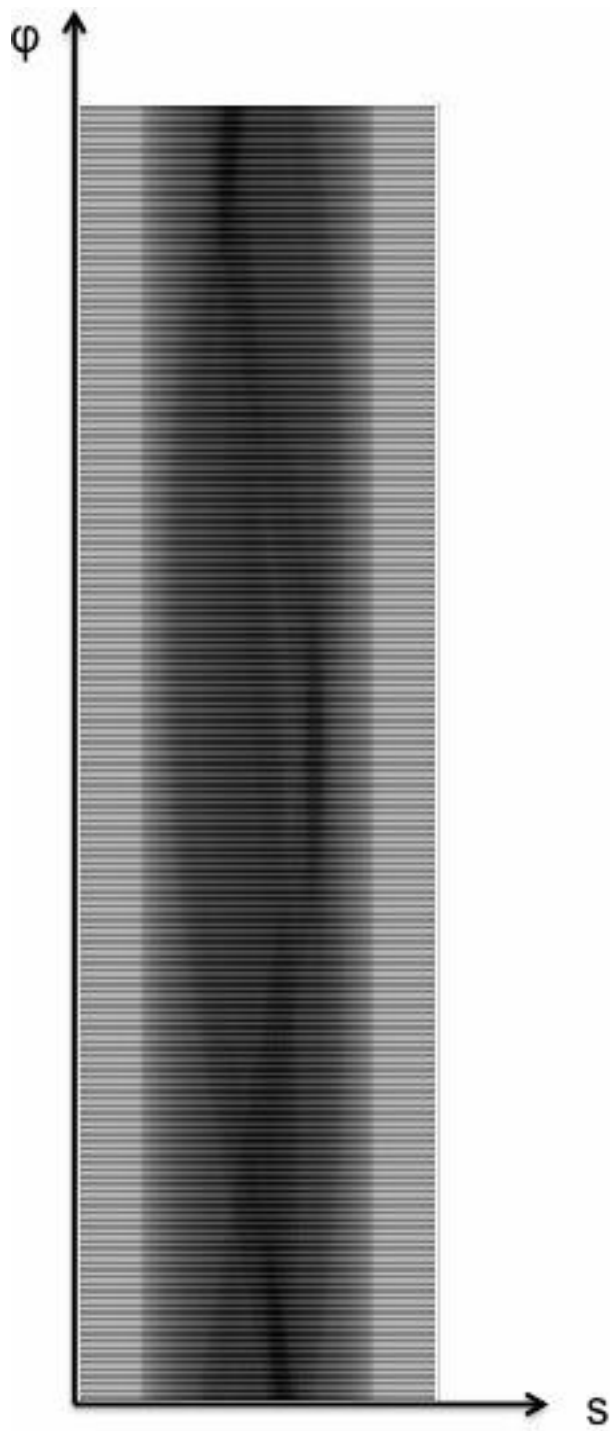
Figure 5.3 Radon Transform for N=5E7
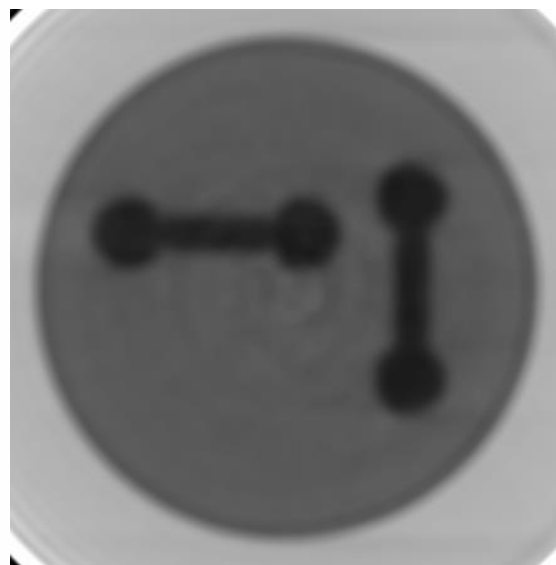
Figure 5.4 Cross-sectional Image
Reconstructed for N=5E7

To see how the number of particles affects the image, I further increased the number of particles to 1E8, keeping the geometry set up same. Increasing the number of particles result in better cross-sectional image. Figure 5.5 and Figure 5.6 shows the results of this simulation.

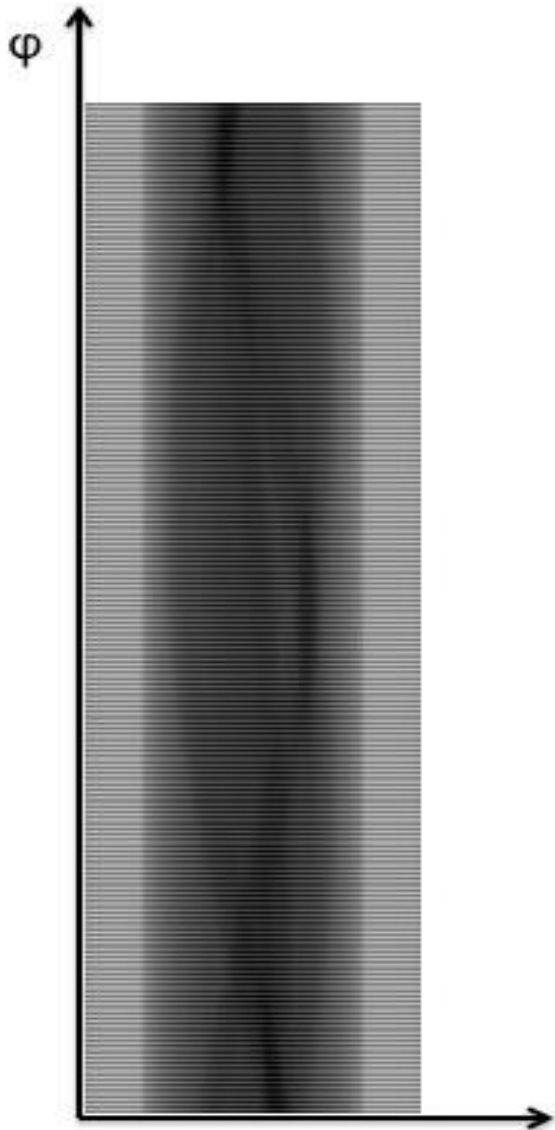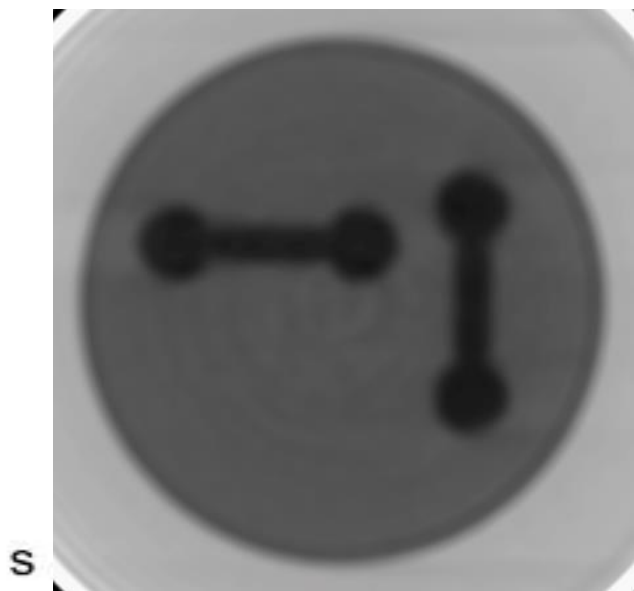
Figure 5.5 Radon Transform for N=1E8

Figure 5.6 Cross-sectional Image Reconstructed for N=1E8

A careful examination of the Radon transform plots of three examples shows that the contrast is getting better with increasing initial number of photons. It can be also seen in the cross-sectional images that by increasing the number of photons, the image gets better. The circular bone in the geometry is more blurred; the reason behind it could be the averaging of pixel values in bone and surrounding water. This artifact can be removed by making pixels of smallest possible size, but that will give rise to new artifacts. In this case, 0.25 centimeters was the adequate size of pixels to get image of good resolution.

Effective Dose Calculation

Although computed tomography is providing many clinical benefits, it results in significant effective radiation dose in patients. Average effective doses for computed tomographic examinations are approximately 2-20mSv [20]. I estimated the effective dose for different number of particles generated, N, using a different FLUKA input file (Appendix D). After applying appropriate fluence to dose conversion coefficients inside the user-routine, the effective dose value returned by FLUKA output is "1.5049E-02 pSv" per unit particle for one angle. As the patient is irradiated from all around, the output value is multiplied by 360 to estimate correct effective dose value.

The results for effective dose for N= 1E7 particles is:

(1.5049E-2)*(1E-12)*(1E+7)*360

=5.418E-5 Sv or 0.054 mSv,

where the factor 1E-12 is to convert pSv into Sv and 1E7 is multiplied to find total effective dose for total number of particles.

Similarly, the effective dose for 5E7 number of particles is 0.27 mSv, for 1E8 is 0.54 mSv, and for 1E9 is 5.4 mSv. The main purpose of calculating the effective dose was to reconstruct images with the lowest possible dose. These calculations could give an idea of how the effective dose and image quality are related. The increase in the effective dose by the increasing number of photons suggests that there is always a trade-off between radiation risks and image quality. It is very important to get an image of reasonable quality with minimum dose.

CHAPTER VI

CONCLUSIONS

X-ray computed tomography is a non-destructive technique for visualizing the interior of the body without the superposition of over- and under-lying organs. In the last two decades, it has become the first exam of choice for some diagnoses because of the advancements in the CT process. In my research project I investigated the image reconstruction by simulating the CT process using FLUKA code and finding the effective dose received by body during the CT process.

For image reconstruction I used a back projection algorithm. The Radon transform and its inverse provide the mathematical basis of filtered back projection method for reconstructing tomographic images using the measured projection data values. I simulated the Radon transform by dividing the number of measured photons by the number of incident photons and then taking the negative logarithm. The sinograms (Figure 5.1,5.3,5.5) for three different values of number of particles, N, were obtained using the Radon transform simulations. To obtain the original image from a sinogram I used the inverse Radon transform in Mathematica software. The cross sectional image of the original geometry (Figure 4.2) was reconstructed for different number of particles as shown in Figures 5.2, 5.4, and 5.6. These images are of reasonable resolution. The image becomes clearer with the increase in the number of incident particles. The noise in the image could be due to the scattered photons reaching the detector. These lower energy photons can be avoided by filtered back projection algorithm. FLUKA code can be used to filter out the photons of lower energy, but it is computationally very expensive in terms of time.

Next, I calculated the effective dose for different reconstruction processes. The quality of the image and the value of the effective dose during the reconstruction process are related to each

36

other. It is very important to reconstruct an image of acceptable quality with the least possible effective dose. The effective dose for N=1E7, 5E8, 1E8, 1E9 number of particles was estimated to be 0.054 mSv, 0.27 mSv, 0.54 mSv, and 5.4 mSv, respectively. The simulation for 1E9 number of particles would take long time, and it was not performed. Although the number of incident photons is not the only factor that influences the effective dose and the image quality, the increase of the effective dose with the increase of the number of incident photons suggests that a high-resolution image comes with high radiation risk to the patient.

The main aim of my research work was to build a relationship between the output of FLUKA code and the CT image reconstruction process. These images could be further improved by filtering the energy of the radiation in the filtered back projection algorithm. The images reconstructed for the geometry I used are of good resolution, but as FLUKA is not a specialized code for CT imaging process, it may not be ideal for good images for smaller organs with similar density. Using filters for X-ray energy can help seeing the details in the images of smaller organs. For future research it would be interesting to see how the slice thickness, the energy of X-rays, the pixel size and most importantly, filtering the energy of radiation helps minimizing the effective dose to the patient without a loss of image quality.

APPENDICES

APPENDIX A

FLUKA INPUT

The FLUKA input consists in a text file that contains a sequence of option lines often

called "cards". Each card contains one keyword, six floating point values, called "WHAT" and

the one character string called "SDUM". The keyword gives the information about the type of

card. The WHATs are the indices corresponding to a material, a type of particle, and a region.

The keywords in SDUM are to give some name to cards (e.g. PHOTON, to say photon beam) or

to declare features such as PRECISION. All WHATs and SDUMs are not necessarily used.

```
*...+... 1....+....2....+....3....+...4....+....5....+....6....+....7....+..8
 TITLE
Reconstructing image using rectangular X-ray beam.
*...+... 1....+....2....+....3....+...4....+....5....+....6....+....7....+..8
GLOBAL      2000.    -1.    0.0     0.0     0.0
```

FLUKA input starts with TITLE card, followed by one line of text that is useful reminder

of what the corresponding file is about. The GLOBAL card is used to set some important

parameters, such as, maximum number of regions (WHAT (1)), to declare if the run is analog

(WHAT (2) < 0) or biased (WHAT (2) >1), to declare about the use of DNEAR (WHAT (3))

variable. DNEAR stands for distance between the current particle position and the nearest

boundary. WHAT (4) flags request various types of inputs. If WHAT (4) is zero it means its

ignored.

```
*...+... 1...+....2....+....3....+...4....+...5....+....6....+....7....+....8
DEFAULTS                              PRECISIO
```

DEFAULTS card sets FLUKA defaults those are suitable for a specified kind of particles.

No WHAT (1-6) is used in this card and SDUM is not allowed to be left blank. PRECISIOn is

used in SDUM in this input file. It activates electromagnetic field, heavy fragment transport,

heavy particle bremsstrahlung, Rayleigh scattering and inelastic form factor corrections to

Compton scattering, photoelectric edge treatment, and many other defaults.

```
BEAM       -14.E-5    0.0         46.    .5          1.0PHOTON
BEAMPOS       0.0    0.0    -40.0
```

BEAM card is used to define several beam characteristics; beam energy, type of beam

divergence (rectangular angular distribution or Gaussian angular distribution). BEAMPOS card

defines the position of beam i.e. co-ordinates of the center of beam spot. In the above example,

BEAM card gives a photon beam of energy 14.E-5 GeV (WHAT (1)); the negative sign signifies

the average beam kinetic energy), with width in x and y directions 46c.m. and 0.5c.m.

respectiviley. Beam is positioned at (0,0, -40) as given in BEAMPOS card.

```
*...+... 1...+....2....+....3....+...4....+...5....+....6....+....7....+....8
ROT-DEFI    200.     0.0    000.   0.0             test
```

This card defines the rotations and translations applied to the bodies in the geometry.

WHAT (1) defines the transformation index and the corresponding rotation axis of rotation. In

my example 200 (i+j*100, where i is index of rotation and j defines axis of rotation) corresponds

to the rotation around y-axis and the index of rotation is 100. ROT-DEFIni card rotates the

bodies within the $Start_transform and $End_transform directives (discussed later).


```
GEOBEGIN                                  COMBNAME
    0     0   Geometry Set-up
RPP bhole     -5000.0 +5000.0 -5000.0 +5000.0 -5000.0 +5000.0
RPP vacum      -1000.0 +1000.0 -1000.0 +1000.0 -1000.0 +1000.0
RPP air       -500.0  +500.0 -500.0  +500.0 -500.0  +500.0
$start_transform  test
RPP body       -21.0 +21.0  -21.0   21.0   -21.0   21.0
RCC body1     0.0   -2.5    0.0   0.0     5.     0.0 14.
RCC body2     0.0   -2.5    0.0   0.0     5.     0.0 13.6
RPP bone      -3.0   3.0   -1.0   +1.0   -8.0   -6.0
RPP bone1      2.0   4.0   -1.0   +1.0    1.0    7.0
RPP BONE2       -5.  -1.0   -1.0   +1.0    3.0    7.0
```

```
RCC bon1        -5.  -2.0  -7.    0.0   4.0   0.0   2.
RCC bon11        3.  -2.0  -1.0   0.0   4.0   0.0   2.
RCC bon2         5.  -2.0  -7.    0.0   4.0   0.0   2.
RCC bon22        3.  -2.0   9.    0.0   4.0   0.0   2.
$end_transform
RPP Detect      -21.  +21.  -.5    .5    60.   61.
END
```

GEOBEGIN card is the beginning of combinatorial input geometry that includes bodies

and regions. It is then preceded by GEOEND card, which means the end of geometry input.

Different body types (RPP, RCC, SPH, XCC, etc.) can be introduced as keywords. The whole

geometry is surrounded by air cavity, then vacuum and then by black hole respectively.

$Start_transform and $End_transform are the directives to define rotation. Bodies in between

these directives will be rotated at an angle defined in ROTDEFni card.

I used rectangular parallelepiped (RPP) and right circular cylindrical (RCC) bodies ,

which are immediately followed by their names (bhole, vacuum, air,body,body1,body2 etc.).

WHATs (1-6) in RPP give the dimensions of the body as follow: x_min, x_max, y_min, y_max,

z_min, z_max respectively. Seven numbers define RCC : V_x,V_y, V_z (coordinates defining

the center of one of the circular faces of cylinder), H_x, H_y, H_z (coordinates defining height

of cylinder) and R, radius of cylinder.

```
* black hole
Blkhole     5 +bhole  -vacum
* vacuum around
Vacc        5 +vacum   -air
* air cavity
Aire        5 +air -body-body2-body1  -Detect
* Body
body        5 +body-body1 -body2 -bone -bone1-bon1-bon11-bon2-bon22-BONE2
.
.
.
bone22      5 +bon22
bone222     5 +BONE2
END
```

41

GEOEND

Before assigning the materials to different regions, it is very important to specify the

regions of the bodies. For example, in above cards (+) sign means the upper limit of the region

and (-) sign means that the region with this sign need to be subtracted. Based on this intersection

of regions, different names are given to different regions, and these names are used for assigning

materials.

```
*..+....1....+....2....+....3....+....4....+....5....+....6....+....7....+....8
MATERIAL                1.85                    Bone_Com
COMPOUND -.063984  HYDROGEN  -.278   CARBON   -0.027 NITROGEN  Bone_Com
COMPOUND -.410016   OXYGEN  -0.002  MAGNESIU   -.07   PHOSPHO Bone_Com
COMPOUND  -0.002   SULFUR  -.147   CALCIUM              Bone_Com
MATERIAL    17.  35.4527  .003214              CHLORINE
MATERIAL    19.  39.0983   .862                POTASSIU
```

Each geometry region is filled with a material and that material is defined by using

material card. Material can be a simple element or a compound. WHATs in material card

specify name, density, material number, atomic number, mass number etc.

```
*..+....1....+....2....+....3....+....4....+....5....+....6....+....7....+..8
*  Assigning materials to Body and Tumor
ASSIGNMA     AIR     body
* External Black Hole
ASSIGNMA   BLCKHOLE  Blkhole
* Air
ASSIGNMA     AIR     Aire
* skull
ASSIGNMA Bone_Com     bod1
ASSIGNMA    WATER     bod2
.
.
.
*  Vacuum
ASSIGNMA   VACUUM     Vacc
* Det
ASSIGNMA   SILICON   DETECTR
```

It is very important to associate a material to each geometry region. ASSIGNMAt card

assigns the materials to different regions. What(1)is the name of material that has to be assigned

and WHAT(2) is the name of the region, to which that material is being assigned.

```
*..+....1....+....2....+....3....+....4....+....5....+....6....+....7...+...8
* Cartesian binning to find number of photons
USRBIN     10.0   PHOTON    50.    21.     .5     61.0
USRBIN     -21.    -.5    60.0   168.     4.     1.0&
```

USRBIN card is used to score the distribution of different quantities. Full definition of

this card requires two cards. WHAT (1) is to define type of binning, in my input I used WHAT

(1) as 10, which means I am using Cartesian binning. WHAT (2) tells the quantity to be scored.

WHAT (3) gives logical output unit (WHAT (3) <0, means unformatted output and >0 means

formatted output). WHATs (4-6) give X_max, Y_max, and Z_max for Cartesian binning and in

the continuation card WHATs (1-3) give X_min, Y_min, and Z_min for respective maximums of

Cartesian geometry. WHAT(4-6) gives number of bins in X,Y, and Z direction. In my input I

have 168 bins in X direction, 4 in Y and 1 in Z direction.

```
RANDOMIZ      1.0
* ..+....1....+....2....+....3....+....4....+....5....+....6....+....7....+....8
START    50000000.
STOP
```

RANDOMIZe card sets the seeds for random number generator. WHAT(1) tells the

logical file unit from which to read the seeds. START card defines the number of histories to be

simulated in a run.

INVERSE RADON TRANSFORM USING MATHEMATICA

As I am using Wolfram Mathematica program to get sinogram from image matrix and to use built in inverse Radon transform function to recover original image, it is very important know about different commands I am using for this purpose.
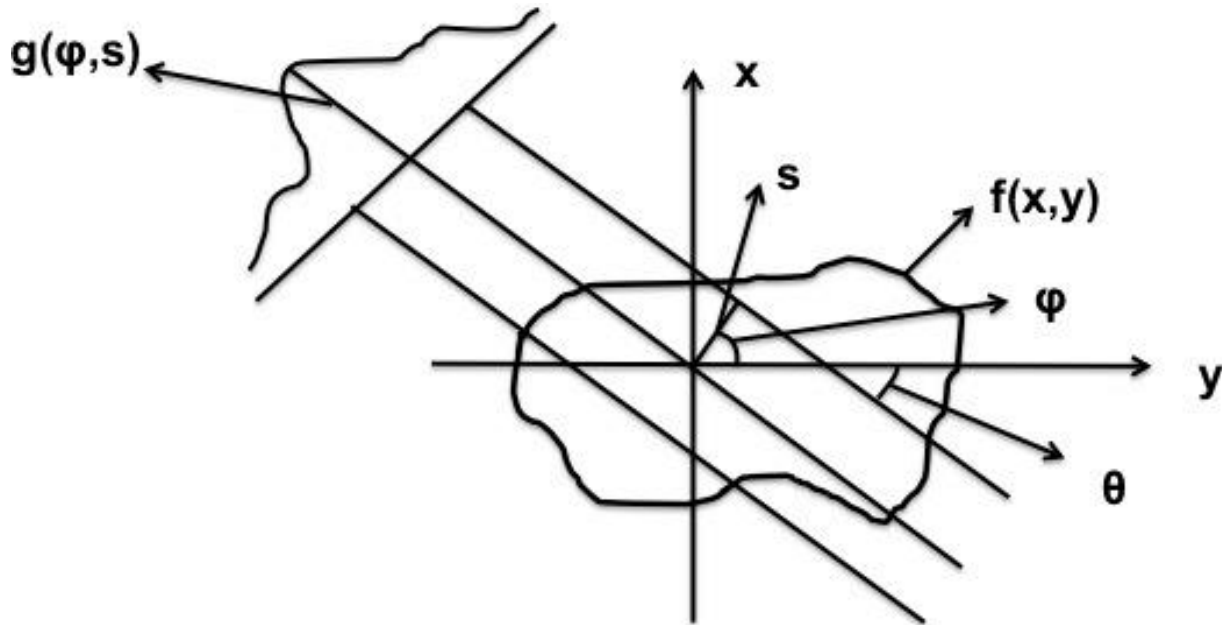

Figure A. Shows the relation between angle of projection φ and θ, the angle used in Radon transform.

In Mathematica, angle θ (Figure A) is used to get sinogram, not angle φ (angle at which body is rotated). It is important to find a relation between angle θ and angle φ. Using simple mathematics, it can be found that the sum of angle θ and φ is 90 degrees:

$$\theta + \varphi = 90^0 \tag{A}$$

This equation (A) is used to find FLUKA output at angles (θ) from -90^0 through 0^0 to $+90^0$. For example, for angle of rotation (φ) 180^0, θ is -90^0.

First, the image matrix is imported to Mathematica and a sinogram is obtained using the command:

ArrayPlot [*Imagematrix*, Mesh □ None]

To reconstruct the original image from a sinogram the inverse Radon function is used as following:

InverseRadon[*Image*, "Filter" □ (# Cos[# Pi]&)]//ImageAdjust

The inverse Radon function finds an approximation of the inverse Radon transform. Since the Mathematica inverse Radon function assumes that columns represents the angles from -90^0 to $+ 90^0$ relative to vertical axis, and the rows represent the distances s to the center of the output, the sinogram is rotated by 90^0 using the command " ImageRotate". The image returned by the inverse Radon function is the square image whose sides have the length equal to the diagonal of the image. Filter options in the command specifies a frequency filter to be applied before computing the back projection. The (#Cos[#Pi]&) filter is a ramp filter multiplied by cosine function. Image Adjust feature is used to adjust the brightness and contrast of the image [22].

EXAMPLE I

A simple geometry was firstly used to check if the method used for reconstruction purpose and the FORTRAN code used to create the image matrix for reconstruction purpose is working correctly or not. The geometry includes two small cubes placed adjacent to each other and surrounded by a bigger cube (as shown in Figure B). The material assigned to the middle black cubes is bone and to the bigger cube is air.
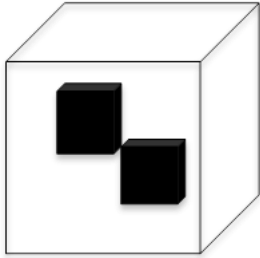

Figure B. Input Geometry

An X-ray beam (width in x direction 46 cm and in y 0.5 cm) of energy 140 keV is simulated to pass through the body, and on the other side is an array of detectors (Figure 4.1). Figure C is the sinogram obtained from FLUKA simulations and Figure D gives the cross-sectional view of original image obtained using the Mathematica software for the inverse Radon transform.
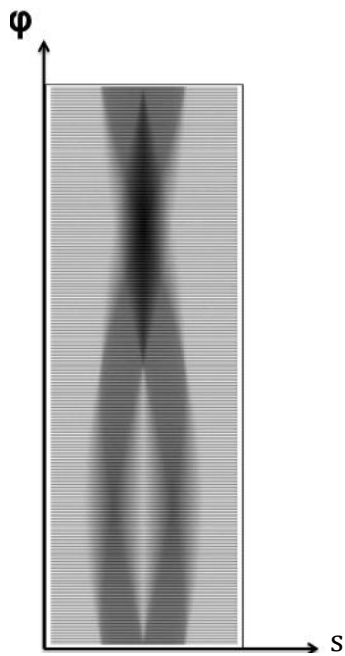
Figure C. Plot of function $-lnN/N_o$ (Radon transform) vs displacement s and angle φ. Lighter regions indicate larger values and darker indicate smaller values.
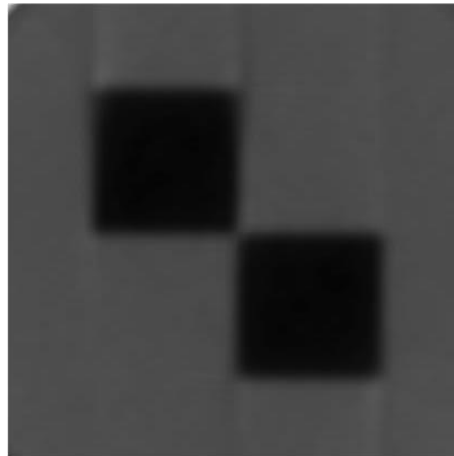

Figure D. Cross-sectional image of body after using inverse Radon transform.

APPENDIX D

DOSE CALCULATION

To find effective dose, few changes were made in the FLUKA input file. A new card,

AUXSCORE, was added in the input for this purpose.

USRBIN   10.   PHOTON   50.   14.   .5   14.0

USRBIN   -14.   -.5   -14.0   1.   1.   1.0&

AUXSCORE   2.   7.   1.   EAP74

AUXSCORE card associates the quantity scored in detectors with dose equivalent

conversion factors. WHAT (1) describes the binning type to be associated with this card. In this

input I used WHAT (1) 2 means USRBIN is associated with AUXSCORE. The number 1 in

WHAT (2) means that the particle to be considered for associated scoring card is photon. Default

values are used for WHATs 5 and 6. Dose conversion coefficients can be described by SDUM.

Set EAP74 in SDUM means Anterior- Posterior irradiation. This set is from ICRP74 and

implemented by using Pelliccioni data calculated with ICRP radiation weighing factors, W_R

(Table 3.1).

The output of the effective dose simulation is:

Total number of particles followed 10000000, for a total weight of 1.0000E+07

The Cartesian binning is used to describe the volume of interest to find effective dose. I

used the slice of thickness (28,1,28) centimeters in (x,y,z) directions respectively to find dose.

Cartesian binning n. "d_eff", generalized particle n. 7

X coordinate: from -1.4000E+01 to 1.4000E+01 cm, 1 bins (2.8000E+01 cm wide)

Y coordinate: from -5.0000E-01 to 5.0000E-01 cm, 1 bins (1.0000E+00 cm wide)

Z coordinate: from -1.4000E+01 to 1.4000E+01 cm, 1 bins (2.8000E+01 cm wide) Data follow

in a matrix A(ix,iy,iz), format (1(5x,1p,10(1x,e11.4)))

accurate deposition along the tracks requested

this is a track-length binning

1.5049E-02

1.5049E-02 is the effective dose in pSv per particle. Effective dose was calculated for different number of photons. The effective dose for 1E7 number of particles is 0.054 mSv, for 5E7 is .27 mSv and for 1E8 is 0.54 mSv (Chapter 5).

APPENDIX E

IMAGE MATRIX

To reconstruct an image, the CT system must segment projection data into tiny sections. An image matrix is a grid that is used to break the data into columns and rows of tiny squares. Each tiny square is called pixel (Figure E.). Each pixel has a width X and length Y, however, it is important that each pixel represents a three-dimensional portion of patient's tissue. So, taking into account the slice thickness, patient data can be represented by voxel (Figure F.).
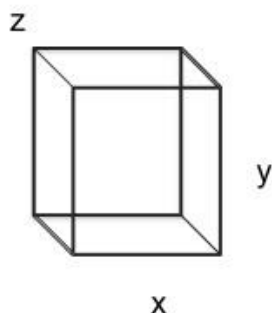

Figure E. Pixel element   Figure F. Voxel element

An image matrix in my work is a matrix of dimensions 168x724, with pixel size 0.25 centimeters. To reconstruct the cross-sectional image with dimensions 42,1,1 centimeters in x, y, z direction respectively I used a detector of the same size of the slice. I further divided the detector into 168,4,1 bins in x, y, z direction respectively to get images of better quality. For each angle of the projection I have 168x4 values, and each value accounts for a number of photons of the X-ray that passes through the body and strikes the detector. Finally, after running the simulation for 181 angles of projection, I used a Fortran code to prepare the image matrix as input for Mathematica.This image matrix is a matrix of of dimension 168x724, with each pixel representing the $-lnN/N_0$ values.

REFERENCES

[1] Bushberg, J. T. (2011). *The essentials physics of medical imaging* (3rd ed.). Philadelphia: Wolters Kluwer Health/Lippincott Williams & Wilkins.

[2] Buzug, T. M. (2008). *Computed tomography from photon statistics to modern cone-beam CT*.   Berlin: Springer.

[3] Cho, Z., Jones, J. P., & Singh, M. (1993). *Foundations of medical imaging*. New York: Wiley.

[4] Guy, C., & Ffytche, D. (2005). *An introduction to principles of medical imaging* (Rev. ed.). London: Imperial College Press.

[5] Herman, G. T. (1980). *Image reconstruction from projections: the fundamentals of computed tomography*. San Francisco: Academic Press.

[6] Iniewski, K. (2009). *Medical imaging principles, detectors, and electronics.* Hoboken,N.J.: Wiley

[7] Jackson, S. A., & Thomas, R. M. (2005). *Cross-sectional imaging made easy.* Edinburgh: Churchill Livingstone.

[8] Kane, S. (2003). *Introduction to physics in modern medicine.* London: Taylor & Francis.

[9] Klein, A., & Godunov, A. (2006). *Introductory to computational physics.* Cambridge:Cambridge University Press.

[10] Manno, I. (1999). *Introduction to the Monte-Carlo method.* Budapest: Akadémiai Kiadó.

[11] Strang, J. G., & Dogra, V. (2007). Body CT secrets. Philadelphia, PA: Mosby Elsevier.

[12] McNitt-Gray, M. F. (2002). AAPM/RSNA Physics Tutorial For Residents: Topics In CT: Radiation Dose In CT. *Radiographics*, *22*(6), 1541-1553.

[13] Brenner, D., & Huda, W. (2008). Effective Dose: A Useful Concept In Diagnostic Radiology? *Radiation Protection Dosimetry*, *128*(4), 503-508.

[14] Welcome to the Canadian Nuclear Safety Commission / Bienvenue au Commission canadienne de sûreté nucléaire. (n.d.). *Welcome to the Canadian Nuclear Safety Commission / Bienvenue au Commission canadienne de sûreté nucléaire*. Retrieved June 19, 2013, from http://nuclearsafety.gc.ca.

[15] Mettler, F. A., Huda, W., Yoshizumi, T. T., & Mahesh, M. (2008). Effective Doses In Radiology And Diagnostic Nuclear Medicine: A Catalog. *Radiology*, *248*(1), 254-263.

[16] Health Physics Society. (n.d.). *Health Physics Society*. Retrieved June 19, 2013, from http://hps.org

[17] Yu, L., & Leng, S. (n.d.). Image Reconstruction Techniques - Image Wisely – Image Wisely. *Radiation Safety in Adult Medical Imaging - Image Wisely*. Retrieved June 19, 2013, from http://www.imagewisely.org/Imaging-Professionals/Medical-Physicists/Articles/Image-Reconstruction-Techniques

[18] https://wiki.engr.illinois.edu/display/BIOE414/Mathematical+Backend

[19] S. Cherry, J. Sorenson and M. Phelps, *Physics in Nuclear Medicine.* Saunders Elsevier Science,   Philadelphia, PA (2003).

[20] Mettler, F. A., Huda, W., Yoshizumi, T. T., & Mahesh, M. (2008). Effective Doses In Radiology And Diagnostic Nuclear Medicine: A Catalog. *Radiology*, *248*(1), 254-263.

[21] A. Ferrari, A. Fasso, J. Ranft and P. Sala, *Fluka: a multi-particle transport code* (2000-2012), URL http://www.fluka.org.

[22] http://www.wolfram.com/mathematica

[23] Saha, G. B. (2012). *Physics and radiobiology of nuclear medicine* (4th ed.). New York: Springer.

[24] http://serc.carleton.edu/research_education/geochemsheets/techniques/CT.html

[25] Dunn, W. L., & Shultis, J. K. (2012).*Exploring Monte Carlo methods*. Amsterdam: Elsevier/Academic Press.

[26] Sobolʹ, I. M. (1994). *A primer for the Monte Carlo method*. Boca Raton: CRC Press.

[27] http://info-fluka-discussion.web.cern.ch/info-fluka-discussion/download/deq2.pdf

[28] http://en.wikipedia.org/wiki/Shepp-Logan_Phantom

[29] http://capone.mtsu.edu/phys4600/Syllabus/CT/Lecture_5/CT-BeamGeometries.jpg